Coastal *Synechococcus* strains can exploit low oxygen habitats

Sylwia Śliwińska-Wilczewska[1,2], Mireille Savoie[1], and Douglas A. Campbell[1,✉]

[1] Department of Biology, Mount Allison University, 53 York St., Sackville, NB, E4L 1C9, Canada

[2] Institute of Oceanography, University of Gdansk, 46 Pilsudskiego St, P81-378, Gdynia, Poland

✉ Correspondence: Douglas A. Campbell <dubhglascambeuil@gmail.com>

Abstract

We found that PhycoErythrin-rich *Synechococcus* achieved faster growth rates (μ), across the spectral bandwidths from 405 – 730 nm, under 2.5 μM [O_2], characteristic of Oxygen Minimum Zones (OMZs), than under 250 μM [O_2], whereas PhycoCyanin-rich strain showed generally similar μ under 2.5 and 250 μM [O_2]. For PhycoCyanin- and PhycoErythrin-rich *Synechococcus*, μ showed also positive linear responses to both Phycobiliproteins:Chlorophyll *a*, and to cumulative diel PSII electron flux, although the relations vary across strain and [O_2]. Electron transport downstream of Photosystem II was generally higher for both PhycoCyanin- and PhycoErythrin-rich strains under 250 μM [O_2], since cyanobacteria show strong capacity for electron flow away from PSII to O_2, particularly under excess excitation. Even though electron transport was faster under 250 μM [O_2], the PhycoErythrin-rich strain showed a higher growth yield of electron transport under 2.5 μM [O_2]. PhycoErythrin-rich *Synechococcus* are currently typically found at greater depths, and lower light, than are PhycoCyanin-rich strains, but we suggest that the PhycoErythrin-rich strains are actually limited to lower light by an interaction

between light and full air-saturated [O_2]. In expanding Oxygen Minimum Zones PhycoErythrin-rich strains will likely exploit higher light niches, across a wider spectral range.

Key words: Colour, niches, OMZs, oxygen concentration, PC-rich strain, PE-rich strain, spectral wavebands, *Synechococcus*

Introduction

Since the mid-20th century, declining oxygen concentrations in regions of the open ocean, and in coastal waters (Breitburg et al. 2018) are affecting productivity, biodiversity, and biogeochemical cycles in marine ecosystems (Keeling et al. 2010). Low oxygen environments in the ocean, termed Oxygen Minimum Zones (OMZ) have expanded to an area equivalent to the European Union, and the global volume of oxygen-free water has quadrupled (Breitburg et al. 2018). It is thus necessary to understand which species will survive and dominate under ongoing and predicted changes in ocean and coastal oxygen concentrations.

Oxygenic picocyanobacteria numerically dominate the phytoplankton across vast tracts of the world's oceans, notably in oligotrophic regions, but also in some coastal ecosystems (Larsson et al. 2014; Śliwińska-Wilczewska et al. 2018a; Aguilera et al. 2023). Oxygen is a product of photosynthesis, and a substrate for reductant consumption, but also has potential to damage Photosystem II (PSII) protein subunits (Andersson et al. 1992). The oxygen evolving complex of PSII can also be directly inactivated by a photon in the UV or blue range directly absorbed by the Mn_4Ca cluster (Hakala et al. 2005; Partensky et al. 2018); therefore, oxygen interacts with spectral band to influence the balance between productive photosynthesis and costly photoinactivations (Murphy et al. 2017). OMZ pose challenges for aerobic organisms (Breitburg et al. 2018), but

picocyanobacteria inhabiting OMZs have genetic adaptations enabling them to tolerate and even thrive in oxygen-depleted environments, such as changes in energy metabolism, antioxidant defense mechanisms, and cellular structures optimized for oxygen scavenging and storage (Ulloa et al. 2012, 2021; Bagby and Chisholm 2015; Partensky et al. 2018; Callieri et al. 2022; Wong et al. 2023).

Picocyanobacteria also show photosynthetic adaptations to spectral wavebands, ranging from short-wavelength blue light (Luimstra et al. 2018), through green and yellow light to long-wavelength red light. Plankton ecologists have long acknowledged that a diverse array of photosynthetic pigments allows cyanobacteria species to exploit different spectral wavebands (Falkowski et al. 2004; Stomp et al. 2007). The ecological success of picoplanktonic *Synechococcus* strains throughout the photic oceanic water column (Flombaum et al. 2013) results in part from diverse strategies to respond to variations in their environment (Scanlan 2012; Doré et al. 2020). The genus *Synechococcus* is genetically diverse and divided into several major clusters. Picocyanobacteria from *Synechococcus* cluster 5, often found in marine, brackish and freshwater environments (Sánchez-Baracaldo et al. 2019; Aguilera et al. 2023), includes sub-clusters of strains rich in phycoerythrin (PE-rich), which imparts a range of orange, reddish, pink, and purple colors, as well as sub-clusters of strains rich in phycocyanin (PC-rich), which color the organism in various shades of blue-green (Stomp et al. 2004). Competition experiments demonstrate that PC-rich and PE-rich strains can coexist in white light but show spectral niche differentiation (Haverkamp 2008; Callieri et al. 2012).

PE-rich strains, with high content of the chromophore phycourobilin (PUB), dominate oligotrophic deep waters where blue light predominates, and deep communities in more mesotrophic marine waters, characterized by blue-green light environments (Stomp et al. 2004;

Haverkamp et al. 2009) are shifting towards PE-rich Synechococcus with more phycoerythrobilin (PEB). Conversely, PC-rich strains prevail near the surface, and in turbid waters where orange and red light dominate. The widespread coexistence of PC-rich and PE-rich picocyanobacteria is observed in waters of intermediate turbidity, such as mesotrophic lakes and coastal seas (Haverkamp 2008; Haverkamp et al. 2009).

Our aim was to test the growth and functional responses of PC-rich and PE-rich *Synechococcus* cultures to the interaction of different oxygen concentrations (250 µM or 2.5 µM [O_2]), and spectral wavebands (405 – 730 nm). We thus empirically answer the question posed by Wong et al. (2023) regarding the sensitivity of modern picocyanobacteria to low levels of O_2 and a wide range of wavebands found across depths and trophic levels.

Materials and methods

Culture condition and experimental setup

Xenic cultures of PC-rich (CCBA_077) and PE-rich (CCBA_127) *Synechococcus* were obtained from the Culture Collection of Baltic Algae (https://ccba.ug.edu.pl/pages/en/home.php) (Latala et al. 2006). *Synechococcus* strains were cultured in Tissue Culture Flasks (VWR International, Cat. No. 10062-872, PA, USA) and transferred biweekly to fresh f/2 media (Guillard 1975) prepared at a salinity of 8 PSU, reflective of their natural brackish habitat. Pre-cultures were maintained in incubators with full air saturated dissolved oxygen concentration [O_2] of 250 µM, 22℃, with a light/dark cycle of 12 hours (h) and Photosynthetically Active Radiation (PAR) of 10 µmol photons $m^{-2}s^{-1}$ from Philips Cool White F14T5/841 Alto, 14 watts, fluorescent bulbs.

Controlled growth experiments were performed using MCMIX-OD PSI Multicultivators (Photon Systems Instruments, Drásov, Czech Republic) set to 22℃. Each of 8 round bottom

cylindrical glass tubes contained 75 mL of f/2 medium and 5 mL of growing pre-culture. These parameters allowed for exponential growth of the cultures from the beginning of the experiment, with little lag phase. Inoculation of culture tubes took place in the afternoon, with a period of low light and then 12 h darkness before a sinusoidal 12 h photoperiod cycle commenced at 07:00 the following morning, with peak PAR of 180 µmol photons $m^{-2}s^{-1}$ reached at 13:00 each day.

Each tube was maintained under an individual combination of one of 7 spectral wavebands centred at 405, 450, 470, 530, 620, 660, or 730 nm and under 250 µM or 2.5 µM [O_2]. Culture tubes were closed with an inert silicone stopper perforated by an aeration input tube extending to the bottom of the culture tube, and a pressure outlet tube. We used aeration with a total gas flow rate of around ~ 140 mL min^{-1} $tube^{-1}$ through a 0.2µm sterile microfilter provided via a G400 gas mixing system (Qubit Systems Inc., Kingston, Ontario, Canada). ~ 250 µM [O_2] was achieved by sparging with lab air (78% N_2, 21% O_2, 1% Ar and 0.05% CO_2). ~ 2.5 µM [O_2] was achieved by sparging with a gas mixture containing 99.95% N_2 and 0.05% CO_2. [O_2] *in situ* was verified using oxygen optodes (PyroScience, Germany) inserted into tubes for real-time measurements (data not presented), with software correction to account for the salinity of the media (8 PSU). The pH of tested cultures remained about 8, with limited fluctuation during the growth experiment (data not presented).

Chlorophyll-specific growth rates

Picocyanobacterial growth was monitored every 5 minutes by automatically recording OD_{680}, OD_{720}, and ΔOD (ΔOD = OD_{680} – OD_{720}) for at least 5 days, independently for each culture tube. The chlorophyll-specific growth rates (µ) were determined by fitting logistic growth curves using a modified Levenberg-Marquardt fitting algorithm (Elzhov et al. 2023) to plots of the

chlorophyll *a* proxy of ΔOD vs. elapsed time (d) for each combination of strain, spectral waveband, and [O_2].

Picocyanobacteria cell counts

Picocyanobacterial cells mL^{-1} were estimated using linear regression models of OD at 680 nm or 720 nm vs. calibration counts of cell suspension densities (cell mL^{-1}) (Table S1). The OD of cultures was measured using MCMIX-OD PSI Multicultivators (Photon Systems Instruments, Drásov, Czech Republic) and cell suspension density measures were conducted using an ImageXpress Pico Digital microscope equipped with CMOS camera and LED+ image autofocus (ImageXpress Pico Automated Cell Imaging System, Molecular Devices, LLC., CA, USA). Culture samples were preserved with 4% glutaraldehyde and kept at -80°C until the microscopy measures. Fixed samples of culture (V = 10 µL) were transferred to surface treated Tissue Culture (TC) black walled 96-well plates (Corning® Falcon® Microplate, MilliporeSigma, Merck, Darmstadt, Germany) with a transparent flat bottom containing 200 µL of f/2 media and centrifuged using a Beckman J-20 centrifuge with a swinging bucket JS-4.3 rotor at 4500 rpm (Beckman Coulter, Brea, California, United States). Cells were imaged with the Cy5 channels (Excitation: 630/40 nm; Emission: 695/45 nm; Dichroic: 655 nm) using selectable confocal geometries, which differentiates cyanobacterial cells from co-occurring heterotrophic bacteria, and counted using a 63x objective in fluorescence imaging modes. Quantitative analysis on images acquired from automated microscopy obtained from 96-well microplates was performed using the CellReporterXpress Image Acquisition and Analysis Software. The representative cell number mL^{-1} was calculated based on the dilution factor and selected count area from each well (Wlodkowic et al. 2022).

137

138 Pigment content and pigment ratio

139 Whole-cell absorbance spectra of picocyanobacteria cells were collected using an integrating
140 cavity spectrophotometer (CLARiTY 17 UV/Vis/NIR, On-Line Instrument Systems, Inc., Bogart,
141 GA, USA) according to the method proposed by Blake and Griff (2012). The sample and reference
142 observation cavities of the spectrophotometer were filled with 8 mL of f/2 medium at salinity 8
143 PSU. After establishing a baseline absorbance spectra from 375 to 710 nm, 4 mL culture medium
144 was replaced with 4 mL of culture in the sample cavity. Pathlength corrected absorbance per cm
145 was calculated using Jávorfi coefficients (Jávorfi et al. 2006). We then conducted estimations of
146 pigment content (μg mL^{-1}) including Chlorophyll *a* (Chl *a*), Carotenoids (Car), Phycoerythrin
147 (PE), Phycocyanin (PC), and Allophycocyanin (APC) from the PC-rich and PE-rich
148 *Synechococcus* cultures. These estimations were based on established linear correlations between
149 pigment content, determined through extraction methods (Strickland and Parsons 1972; Bennett
150 and Bogorad 1973), and absorbance values of individual pigment peaks (Car; 480 nm, PE; 565
151 nm, PC; 620 nm, APC; 650 nm, and Chl *a*; 665 nm) obtained from whole-cell absorbance spectra
152 (Table S2). Additionally, we summed PE, PC, and APC protein to total Phycobiliproteins content.
153 Using whole-cell absorbance spectra of *Synechococcus* cultures, we also estimated
154 Photosynthetically Usable Radiation (PUR; μmol photons $m^{-2}s^{-1}$) according to (Morel 1978).

155

156 PSII effective absorption cross section of PSII, turnover time of PSII
157 photochemistry, and photochemical quenching

158 We harvested 4 mL of picocyanobacteria cultures repeatedly across the growth trajectories
159 for photophysiological characterizations. For the low oxygen cultures, to ensure

160 photophysiological measurements were taken at low O_2 of ~ 2.5 µM, we bubbled gently with N_2
161 from a gas cylinder during measurements. [O_2] was verified in culture samples for
162 photophysiological measurements using oxygen optodes (PyroScience, Germany) inserted (data
163 not presented).

164 We used Fast Repetition & Relaxation chlorophyll fluorescence (FRRf) (Kolber et al. 1998)
165 (Solisense, USA), with a lab built temperature control jacket (22℃), to apply a series of 100
166 excitation flashlets of 1.6 µs to drive saturation of PSII variable fluorescence, followed
167 immediately by logarithmically spaced flashlets to track relaxation of variable fluorescence.
168 Induction/relaxation trajectories were fit using the onboard Solisense LIFT software (Falkowski
169 and Kolber 1993; Kolber et al. 1998).

170 We used a double tap protocol (Xu et al. 2017), where FRRf induction/relaxation trajectories
171 were collected during a rapid actinic light curve sequence increasing in steps of 10 s at 0, 20, 40,
172 80, 160, and 320 µmol photons $m^{-2}s^{-1}$ PAR. We applied 1 s darkness between the sequential 10 s
173 steps of the light response curves, to allow re-opening of PSII immediately after application of the
174 sequential increasing light steps. Flashlets and actinic light were delivered from LED emitters
175 centred at Ex_{445nm}, preferentially exciting chlorophyll; Ex_{470nm}, preferentially exciting
176 phycourobilin (PUB); Ex_{535nm}, preferentially exciting phycoerythrin (PE); or Ex_{590nm},
177 preferentially exciting phycocyanin (PC). Excitation flashlets and actinic light wavebands were
178 matched for each run. These actinic and excitation wavebands in turn approximated 4 of our 7
179 growth light wavebands (450, 470, 530 & 620 nm), allowing us to evaluate *in situ* photosynthetic
180 performance for those culture conditions.

181 Flashlet power delivered to the samples during the 1.6 µs flashlet duration was adjusted to
182 achieve saturation of variable fluorescence; Ex_{445nm} at 60000 µmol photons $m^{-2}s^{-1}$ PAR; Ex_{470nm}

at 30000 µmol photons $m^{-2}s^{-1}$ PAR; Ex_{535nm} at 25000 µmol photons $m^{-2}s^{-1}$ PAR; while for Ex_{590nm} excitation power at 14000 µmol photons $m^{-2}s^{-1}$, calibrated using a quantum sensor (LI-250, LI-COR, Inc.) in the temperature controlled cuvette.

We estimated effective absorption cross section of PSII (σ_{PSII}; nm^2 $quanta^{-1}$); turnover time of PSII photochemistry (τ_{PSII}; µs); and the photochemical quenching coefficient (q_P) using the FRRf induction curves, following (Xu et al. 2017). We fit a model with three τ_{PSII} to describe the re-opening of PSII after closure by the saturating flash train. For subsequent analyses we estimated an average of the three τ_{PSII}, weighted by their respective amplitudes, to describe the overall time to reopen PSII after closure.

PSII electron flux

We calculated (Eq. (1)) an uncalibrated fluorescence based estimator for volumetric electron transport, JV_{PSII}, (k × e^- L^{-1} s^{-1}) under Ex_{445nm}, blue; Ex_{470nm}, blue-green; Ex_{535nm}, green; or Ex_{590nm}, red-orange excitation bands (Oxborough et al. 2012; Boatman et al. 2019; Tortell and Suggett 2021).

$$JV_{PSII} = \frac{\sigma_{PSII}' \times q_P \times I \times F_O}{\sigma_{PSII}} \qquad (1)$$

where σ_{PSII}' is effective absorption cross section for PSII photochemistry under the relevant actinic PAR step (nm^2 $quanta^{-1}$); q_P is an estimate of the fraction of PSII open for photochemistry estimated according to Oxborough and Baker (1997); I is the applied PAR (µmol photons $m^{-2}s^{-1}$); F_O is the minimum fluorescence from a given sample and excitation waveband (relative fluorescence) and σ_{PSII} is the maximum effective absorption cross section for PSII photochemistry from a given sample and excitation waveband (nm^2 $quanta^{-1}$).

We calibrated the JV_{PSII} estimator to absolute rates of electron transport (Eq. (2)) using parallel measures of oxygen evolution (µmol O_2 L^{-1} s^{-1}), captured simultaneously with the FRRf measures, taken below light saturation of electron transport to limit distortion from electron fluxes back to oxygen under super-saturating light (Hughes et al. 2018), using a FireSting robust oxygen probe (PyroScience, Germany) inserted in the cuvette for select Rapid Light Curve (RLC) runs (Table S3).

$$JV_{PSII}(e^{-}\ L^{-1}\ s^{-1}) = \frac{Uncalibrated\ JV_{PSII}(e^{-}\ L^{-1}\ s^{-1})}{Calibration\ slope} \qquad (2)$$

We converted JV_{PSII} (µmol e^- L^{-1} s^{-1}) to JV_{PSII} (µmol e^- µmol Chl a^{-1} d^{-1}) by performing Chl *a* (µg L^{-1}) measurements using Trilogy Laboratory Fluorometer (Turner Designs, Inc., CA, USA) equipped with Chlorophyll In-Vivo Module, on the samples taken for the FRRf measurements.

To generate an index of the ratio of Chl *a* : PSII we divided PSII electron transport (e- $PSII^{-1}$ s^{-1}) by JV_{PSII} (e- Chl^{-1} s^{-1}), both estimated under Ex_{445nm}, with units cancelling to Chl *a* : PSII. Since the number of Chl *a* directly associated with the core of PSII is fixed, variations in Chl *a* to PSII reflect changes in the PSI:PSII ratio, and possibly the presence of other chl-containing complexes.

Statistical analysis

We used R version 4.3.0 (R Core Team 2023) running under RStudio (Posit team 2022). We performed three-way factorial ANOVA (*aov()* function; R Base package) to determine whether strain, growth waveband, and [O_2] significantly influence the chlorophyll-specific growth rate (µ; d^{-1}; Table S4) or pigment content (Table S5). We also performed three-way factorial ANOVA (*aov()* function) to determine whether strain, Actinic PAR, and [O_2] significantly influence the

responses of σ_{PSII} (Table S6); τ_{PSII} (Table S7); q_P (Table S8); or JV_{PSII} (Table S9) to increasing light. We fit the light response curves of JV_{PSII} with a three parameter model (Harrison and Platt 1986) using (Elzhov et al. 2023) for *nlsLM()* function. Three-way factorial ANOVA (*aov()* function; R Base package) was performed to determine whether strain, growth waveband, and $[O_2]$ significantly influence Chl *a* to PSII (Table S10).

We used *t*-tests of linear regressions to compare data across different strains and $[O_2]$ for a given growth waveband, for chlorophyll-specific growth rate vs. Phycobiliproteins to Chl *a* ratio (Table S11). We also performed *t*-tests of linear fits to compare data across different strains and $[O_2]$ in situations in which cultures were excited by, and growing in, corresponding growth wavebands of 450, 470, 530, or 620 nm, for chlorophyll-specific growth rate vs. JV_{PSII} (Table S12). Statistical differences for all analyses were determined at significance level $\alpha = 0.05$.

The manuscript was prepared as a Rmarkdown document (Handel 2020) with figures plotted using ggplot2 (Wickham 2016) and patchwork (Pedersen 2024) packages. All metadata, data, and code is available on GitHub (https://github.com/FundyPhytoPhys/BalticO2).

Results

Chlorophyll-specific growth rates across $[O_2]$, spectral wavebands, and strains

We used logistic curve fits (Fig. S1) to determine chlorophyll-specific growth rates (μ; d^{-1}) for PC-rich and PE-rich cultures of *Synechococcus* grown under spectral wavebands centred at 405, 450, 470, 530, 620, 660, or 730 nm, and $[O_2]$ of 250 µM or 2.5 µM (Fig. 1). Growth curves, tracked as OD_{680}, OD_{720}, ΔOD and logistic fits of ΔOD vs. elapsed time are shown in Fig. S1 in Supplementary materials. Cell-specific growth rates (μ) were also determined using OD_{720} (Fig. S2). Strain, growth waveband, $[O_2]$, and their interactions, significantly affected μ (Table S4).

PC-rich and PE-rich *Synechococcus* grow under 2.5 μM [O_2], across the range of tested spectral wavebands from 405 – 730 nm. In contrast, under 250 μM [O_2], the PC-rich strain failed to grow under 405 nm, while the PE-rich strain failed to grow under 405, 450, and 730 nm. The PC-rich strain showed generally similar growth rates under 2.5 and 250 μM [O_2], across tested spectral wavebands (nm). In contrast the PE-rich strain achieved faster growth rates under 2.5 μM [O_2] than under 250 μM [O_2].

PC-rich *Synechococcus* showed a peak in growth rate under both [O_2] and red light of 620 or 660 nm, absorbed by phycocyanin and chlorophyll. Under 2.5 μM [O_2] the PE-rich strain showed high growth rates under 530 nm – 660 nm absorbed by phycoerythin, phycocyanin, and chlorophyll; while under 250 μM [O_2], the PE-rich strain showed the highest growth rate under green light of 530 nm absorbed by phycoerythrin.

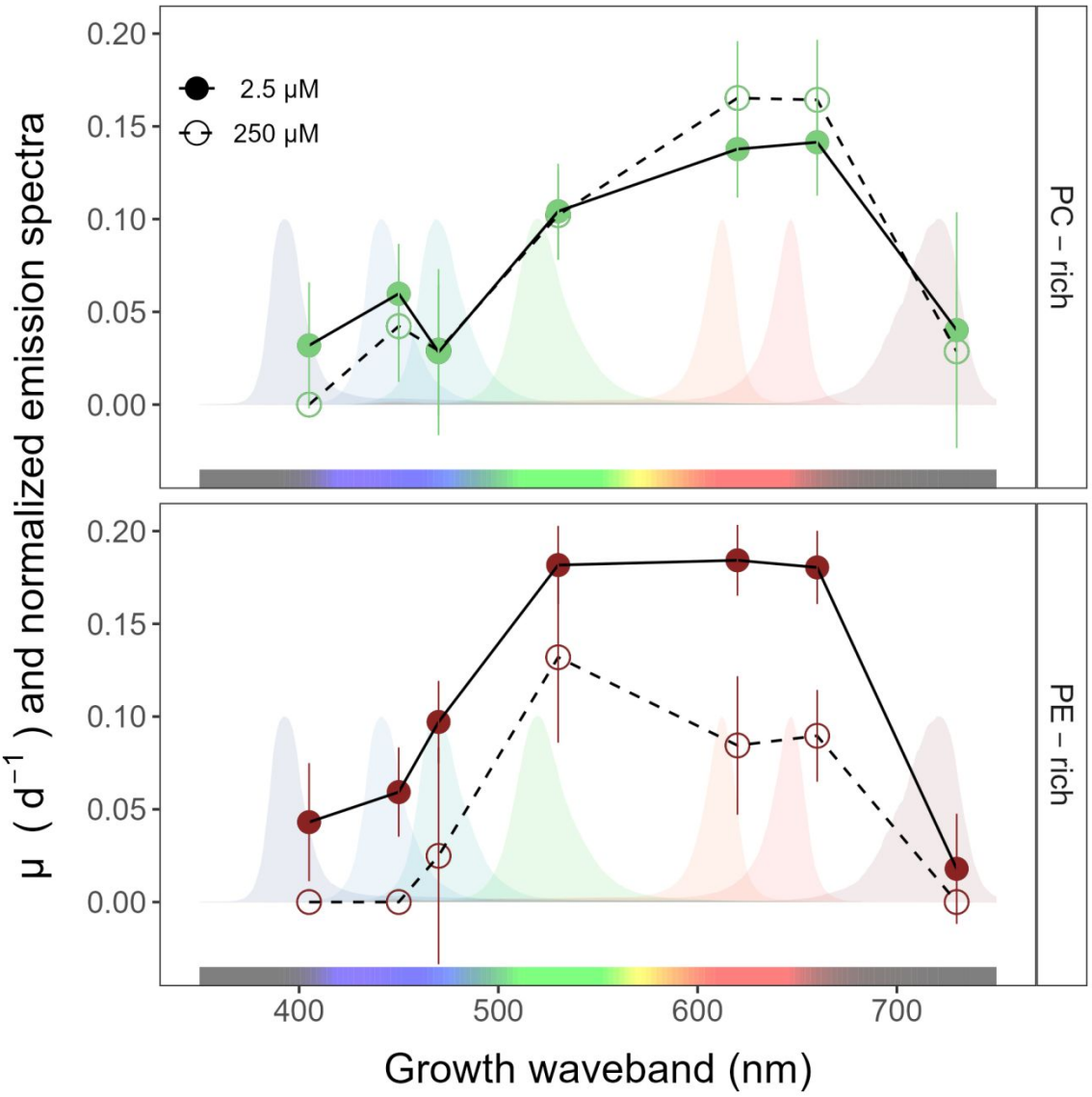

263

264 **Fig.** 1: Chlorophyll-specific growth rates (µ; d^{-1}) vs. growth waveband (nm, shaded regions).
265 Growth rates (± SE) were estimated from logistic fits of chlorophyll proxy $OD_{680} - OD_{720}$ (ΔOD)
266 vs. elapsed time (Fig. S1), for PC-rich (green circle) and PE-rich (red circle) cultures of
267 *Synechococcus* grown at spectral wavebands of 405, 450, 470, 530, 620, 660, or 730 nm, and [O_2]
268 of 250 µM (open symbols and dashed line) or 2.5 µM (closed symbols and solid line).

269

Pigment content and pigment ratio across [O_2], spectral wavebands, and strains

Fig. 2*a* presents Chlorophyll *a* (Chl *a*), Phycobiliproteins (Phyco), or Carotenoids (Car) content (pg cell $^{-1}$) vs. growth waveband (nm) for PC-rich and PE-rich cultures of *Synechococcus* grown at spectral wavebands centred at 405, 450, 470, 530, 620, 660, or 730 nm and 250 or 2.5 µM [O_2]. We also calculated the Car to Chl *a* ratio, and the ratio of the sum of Phycobiliproteins to Chl *a* (µg:µg) for each strain (Fig. S3). Moreover, phycobiliproteins:Chlorophyll *a* ratio (µg:µg) and chlorophyll-specific growth rates (µ; d^{-1}) vs. Photosynthetically Usable Radiation (PUR, µmol photons $m^{-2}s^{-1}$) for PC-rich and PE-rich cultures of *Synechococcus* grown at spectral wavebands of 405, 450, 470, 530, 620, 660, or 730 nm and 250 µM [O_2] or 2.5 µM [O_2] are presented in Fig. S4.

To focus on the responses of growing cells, we omit pigmentation data from those PE-rich cultures which showed negligible growth under 405, 450, 730 nm and 250 µM [O_2]; and from those PC-rich cultures which showed negligible growth under 405 nm and 250 µM [O_2].

Strain, growth waveband, [O_2], and their interactions, significantly affected cell-specific Chl *a*, Phycobiliproteins, and Car content (Table S5). For the PC-rich strain, the highest Chl *a*, Phycobiliproteins, and Car contents were recorded after growth under 730 nm. The phycobiliproteins content was higher under 250 µM [O_2] than under 2.5 µM [O_2] for the PC-rich strain. In contrast, for PE-rich *Synechococcus*, phycobiliproteins content was significantly lower under 250 µM [O_2] than under 2.5 µM [O_2], with the highest phycobiliproteins content under 620 nm and 2.5 µM [O_2].

Chlorophyll-specific growth rates (µ; d^{-1}) show positive linear responses to the Phycobiliproteins:Chlorophyll *a* ratio (µg:µg), for both PC-rich and PE-rich *Synechococcus* (Fig. 2*b*), although the relations vary across strain and [O_2] (Table S11).

293

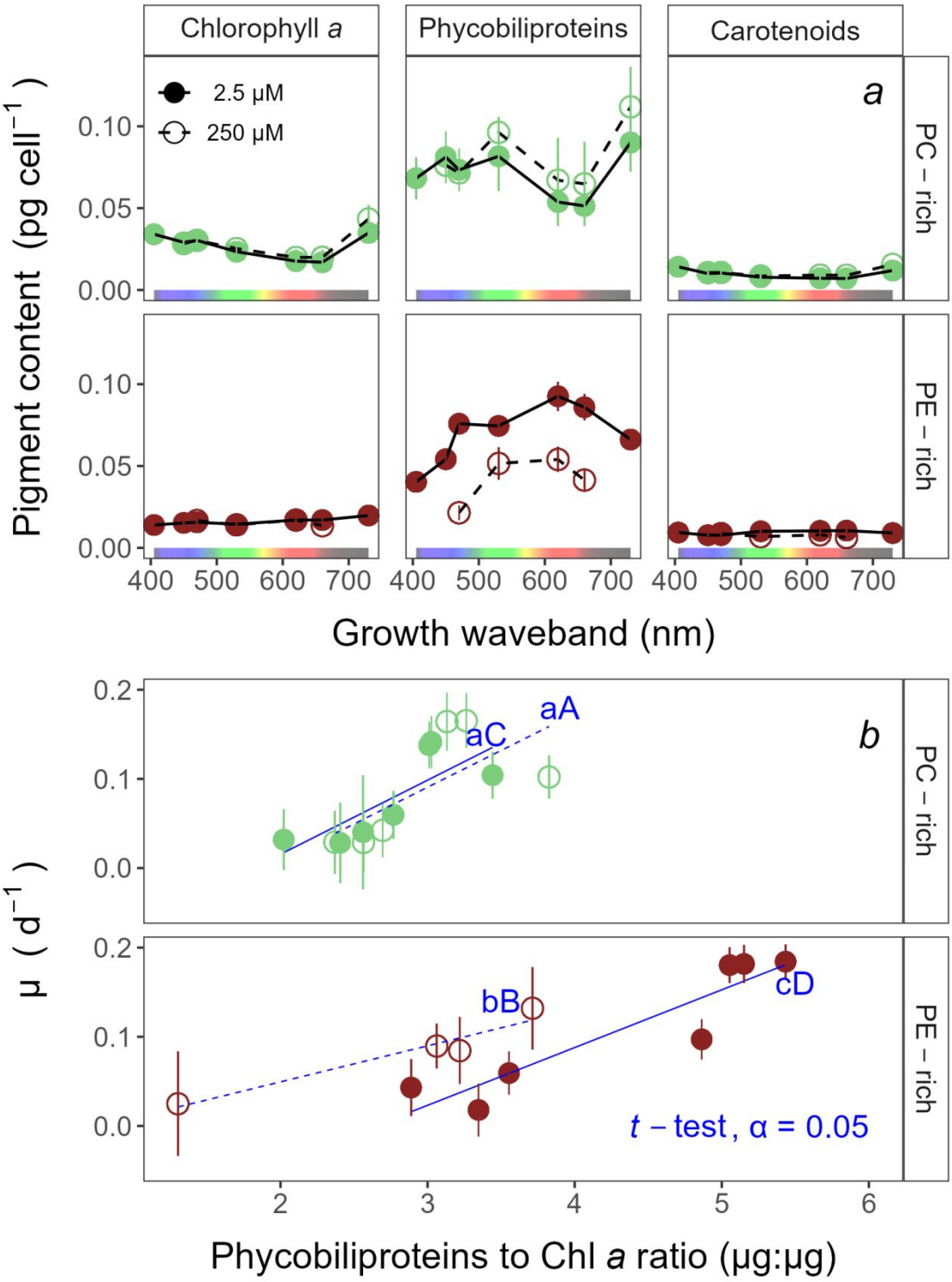

294

295 **Fig.** 2: Pigment content (pg cell $^{-1}$) vs. growth waveband (nm) (*a*) and Chlorophyll-specific growth

296 rates (µ; d^{-1}) vs. Phycobiliproteins:Chlorophyll *a* ratio (µg:µg) (*b*) for PC-rich (green circle) and

297 PE-rich (red circle) cultures of *Synechococcus* grown at spectral wavebands of 405, 450, 470, 530,
298 620, 660, or 730 nm and 250 μM [O_2] (open symbols and dashed line) or 2.5 μM [O_2] (closed
299 symbols and solid line). Data not presented for those PE-rich cultures which showed negligible
300 growth under 405, 450, 730 nm and 250 μM [O_2]; nor for those PC-rich cultures which showed
301 negligible growth under 405 nm and 250 μM [O_2]. Blue lines show linear model fit for data from
302 each strain and [O_2] (solid for 2.5 μM [O_2] or dashed for 250 μM [O_2]) across spectral wavebands.
303 Different blue lowercase letters indicate statistically significant differences between the fit models
304 for different [O_2] within a given strain. Different blue uppercase letters indicate statistically
305 significant differences between the fit models for different strains within a given [O_2] (*t*-test; $p <$
306 0.05).
307

308 Effective absorption cross sections, turnover times, and photochemical quenching of
309 PSII across [O_2], spectral wavebands, and strains

310 Light response curves of effective absorption cross section of PSII (σ_{PSII}; nm^2 $quanta^{-1}$);
311 turnover time of PSII photochemistry (τ_{PSII}; μs); and the photochemical quenching coefficient (q_P)
312 vs. Actinic PAR (μmol photons $m^{-2}s^{-1}$) (Fig. 3*a*-*c*) are shown for PC-rich and PE-rich cultures
313 grown in, and excited by, corresponding wavebands of 450, 470, 530, or 620 nm, at 250 μM or
314 2.5 μM [O_2]. We omit functional data determined for those PE-rich cultures which showed
315 negligible growth under 405, 450, 730 nm and 250 μM O_2; and for those PC-rich cultures which
316 showed negligible growth under 405 nm and 250 μM O_2. In the Supplementary materials (Fig S5-
317 S7), we also show the light response curves for all available excitation (Ex_{445nm}, blue; Ex_{470nm},
318 blue-green; Ex_{535nm}, green; or Ex_{590nm}, orange) and growth waveband (450, 470, 530, or 620 nm)
319 cross-combinations.

320 σ_{PSII} (Fig. 3*a*), a measure of excitation driving PSII photochemistry, was low and shows little
321 change with increasing actinic light during excitation through chlorophyll at Ex_{445nm}. For the PC-
322 rich strain, under orange excitation at Ex_{590nm}, σ_{PSII} showed an initial small increase from darkness
323 to the growth light level, followed by a mild decrease with increasing Actinic PAR, and was higher
324 at 250 μM [O_2] compared to 2.5 μM [O_2]. For the PE-rich strain, we again see a small increase
325 from darkness to the growth light level, followed by a decrease in σ_{PSII} with increasing Actinic
326 PAR. Moreover, for the PE-rich strain σ_{PSII} was higher in low [O_2] conditions than in high [O_2]
327 conditions. Strain, Actinic PAR, and [O_2] significantly influenced σ_{PSII} under excitation at Ex_{590nm}
328 (Table S6).

329 For the PC-rich strain, across the excitation wavebands tested, τ_{PSII} showed an acceleration
330 (decrease) from darkness to growth light Actinic PAR (Fig. 3*b*), to a plateau of ~ 800 μs. PE-rich
331 strains, on the other hand, showed a progressive acceleration (decrease) with increasing Actinic
332 PAR under excitation at Ex_{470nm}, Ex_{535nm}, or Ex_{590nm}, declining towards ~ 400 μs under Ex_{590nm}.
333 Thus, the PE-rich strain showed more capacity to remove electrons from PSII. τ_{PSII}, was generally
334 faster (smaller) for both PC-rich and PE-rich strains under 250 μM [O_2]. Strain, Actinic PAR, and
335 [O_2] significantly affected τ_{PSII} at Ex_{470nm}, Ex_{535nm} and Ex_{590nm} (Table S7).

336 q_P, a measure of the fraction of PSII available for photochemistry, showed a strong decrease
337 with increasing Actinic PAR across the excitation wavebands tested (Fig. 3*c*). q_P generally
338 remained higher for both PC-rich and PE-rich strains under 250 μM [O_2]. Strain, Actinic PAR,
339 and [O_2] significantly affected q_P at Ex_{470nm}, Ex_{535nm}, and Ex_{590nm} (Table S8).

340

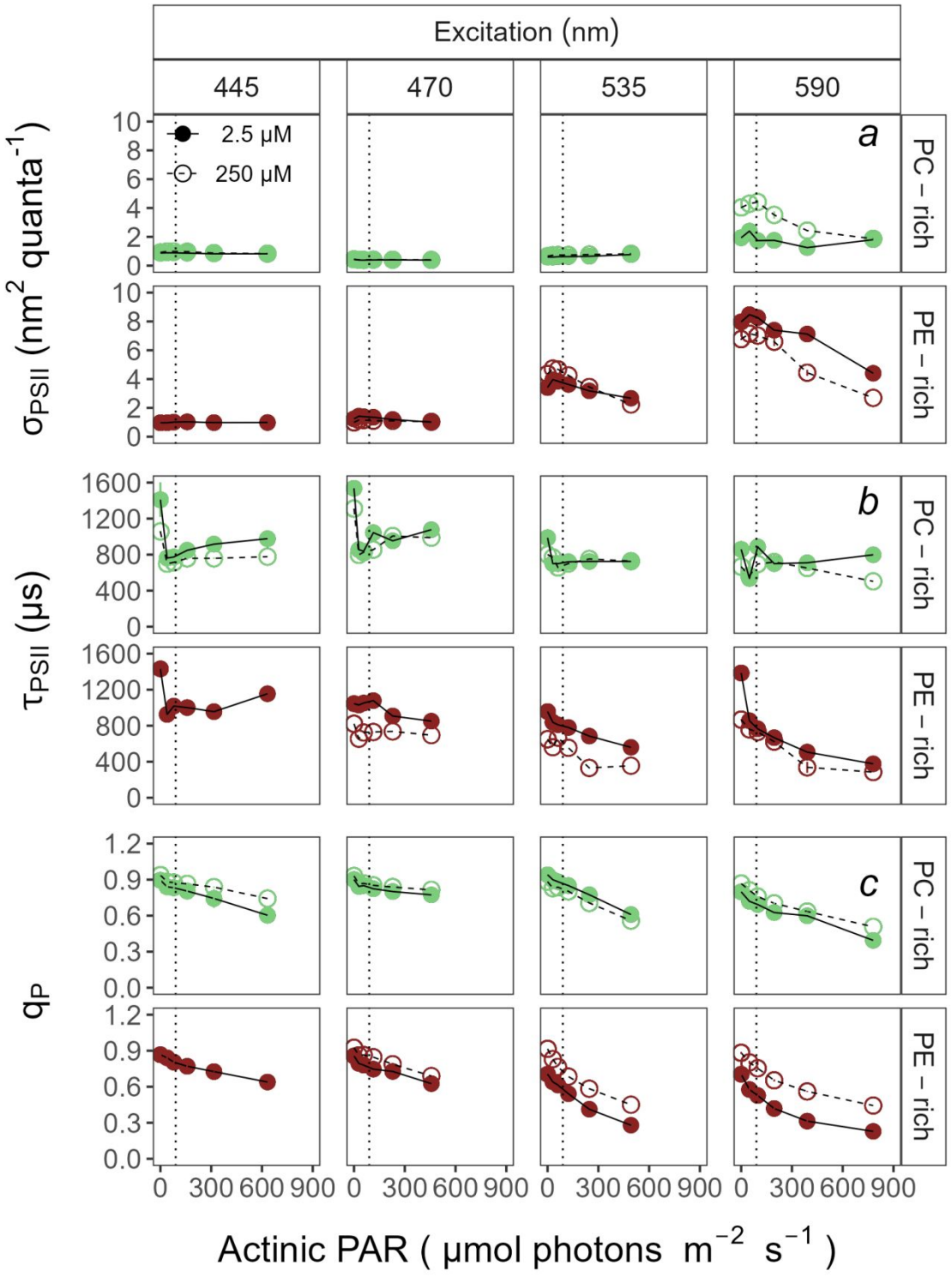

341

342 **Fig.** 3: Effective absorption cross section of PSII (σ_{PSII}; nm^2 quanta^{-1}) (*a*); turnover time of PSII

343 photochemistry (τ_{PSII}; µs) (*b*); or photochemical quenching coefficient (q_P) (*c*) vs. Actinic PAR

(μmol photons $m^{-2}s^{-1}$). Parameters were estimated using FRRf induction curves with excitation (columns) at Ex_{445nm}, blue; Ex_{470nm}, blue-green; Ex_{535nm}, green; or Ex_{590nm}, orange; for PC-rich (green circle) or PE-rich (red circle) cultures of *Synechococcus*. Data show situations in which cultures were excited by, and growing in, corresponding growth wavebands of 450, 470, 530, or 620 nm and 250 μM [O_2] (open symbols and dashed line) or 2.5 μM [O_2] (closed symbols and solid line). The vertical lines show half diel peak PAR growth light of 90 μmol photons $m^{-2}s^{-1}$. Data not presented for those PE-rich cultures which showed negligible growth under 405, 450, 730 nm and 250 μM [O_2]; nor for those PC-rich cultures which showed negligible growth under 405 nm and 250 μM [O_2].

PSII electron flux across [O_2], spectral wavebands, and strains

PSII electron flux (JV_{PSII}) measures the generation of reductant available to support biosynthetic assimilation and growth. JV_{PSII} was estimated using FRRf inductions with excitation at Ex_{445nm}, Ex_{470nm}, Ex_{535nm}, or Ex_{590nm}, corresponding to growth wavebands of 450, 470, 530, or 620 nm and 250 μM or 2.5 μM [O_2]. To focus on responses of growing cells, we do not present JV_{PSII} data for those PE-rich cultures which showed negligible growth under 405, 450, 730 nm and 250 μM O_2; nor for those PC-rich cultures which showed negligible growth under 405 nm and 250 μM O_2. PSII electron flux (JV_{PSII}; μmol e^- μmol Chl a^{-1} s^{-1}) vs. Actinic PAR (μmol photons $m^{-2}s^{-1}$) estimated using FRRf induction curves with excitation at Ex_{445nm}, blue; Ex_{470nm}, blue-green; Ex_{535nm}, green; or Ex_{590nm}, orange; for PC-rich or PE-rich cultures of *Synechococcus* grown at spectral bandwidths of 450, 470, 530, or 620 nm and O_2 concentrations of 250 μM or 2.5 μM are also presented (Fig. S8).

Light response curves of PSII electron flux (JV_{PSII}; µmol e^- µmol Chl a^{-1} s^{-1}) vs. Actinic PAR (µmol photons $m^{-2}s^{-1}$) are shown in Fig. 4*a*. For the PC-rich strain, under all tested excitations (Ex_{445nm}, Ex_{470nm}, Ex_{535nm}, or Ex_{590nm}), JV_{PSII} increased with increasing Actinic PAR, and did not fully saturate across the range of tested actinic PAR. Under all excitations, except Ex_{590nm}, JV_{PSII} was higher at 2.5 µM [O_2] compared to 250 µM [O_2] for the PC-rich strain. Conversely, for the PE-rich strain, JV_{PSII} under Ex_{470nm}, Ex_{535nm}, or Ex_{590nm} was higher at 250 µM [O_2] compared to 2.5 µM [O_2]. Moreover, for the PE-rich strain, JV_{PSII} plateaued above ~90 µmol photons $m^{-2}s^{-1}$ under Ex_{535nm}, or Ex_{590nm} for both low and high [O_2]. Strain, Actinic PAR, and [O_2] significantly influence JV_{PSII} under some of the tested excitations (Table S9), but JV_{PSII} for cultures grown under, and excited through, Ex_{445nm}, absorbed by chlorophyll, shows no difference between low and high [O_2] with increasing actinic light.

Fig. 4*b* presents linear regressions between chlorophyll-specific growth rates (µ; d^{-1}) and cumulative diel PSII electron flux (JV_{PSII}; µmol e^- µmol Chl a^{-1} d^{-1}) measured under half (90 µmol photons $m^{-2}s^{-1}$) of the diel peak PAR growth light. µ (d^{-1}), as expected, was positively correlated with JV_{PSII}, with slopes significantly greater than 0. [O_2] significantly influences the linear regressions between chlorophyll-specific growth rates and PSII electron flux for both PC-rich and PE-rich strains of *Synechococcus* ($p < 0.05$, Table S12). In the PC-rich strain higher [O_2] increases the growth yield of electron transport. In contrast, the PE-rich strain, under higher [O_2], decreases the growth yield of electron transport. However, the regressions for a given [O_2] are not significantly different between the two strains ($p > 0.05$, Table S12).

Strain, actinic PAR waveband, and [O_2] significantly influence Strain, Actinic PAR, and [O_2] significantly influence our metric of Chl *a* : PSII (Fig. S9, Table S10), with Chl *a* : PSII higher

388 under 250 than under 2.5 μM [O_2] in the PC-rich strain, and Chl *a* : PSII generally lower in the
389 PC-rich stain compared to the PE-rich strain.
390

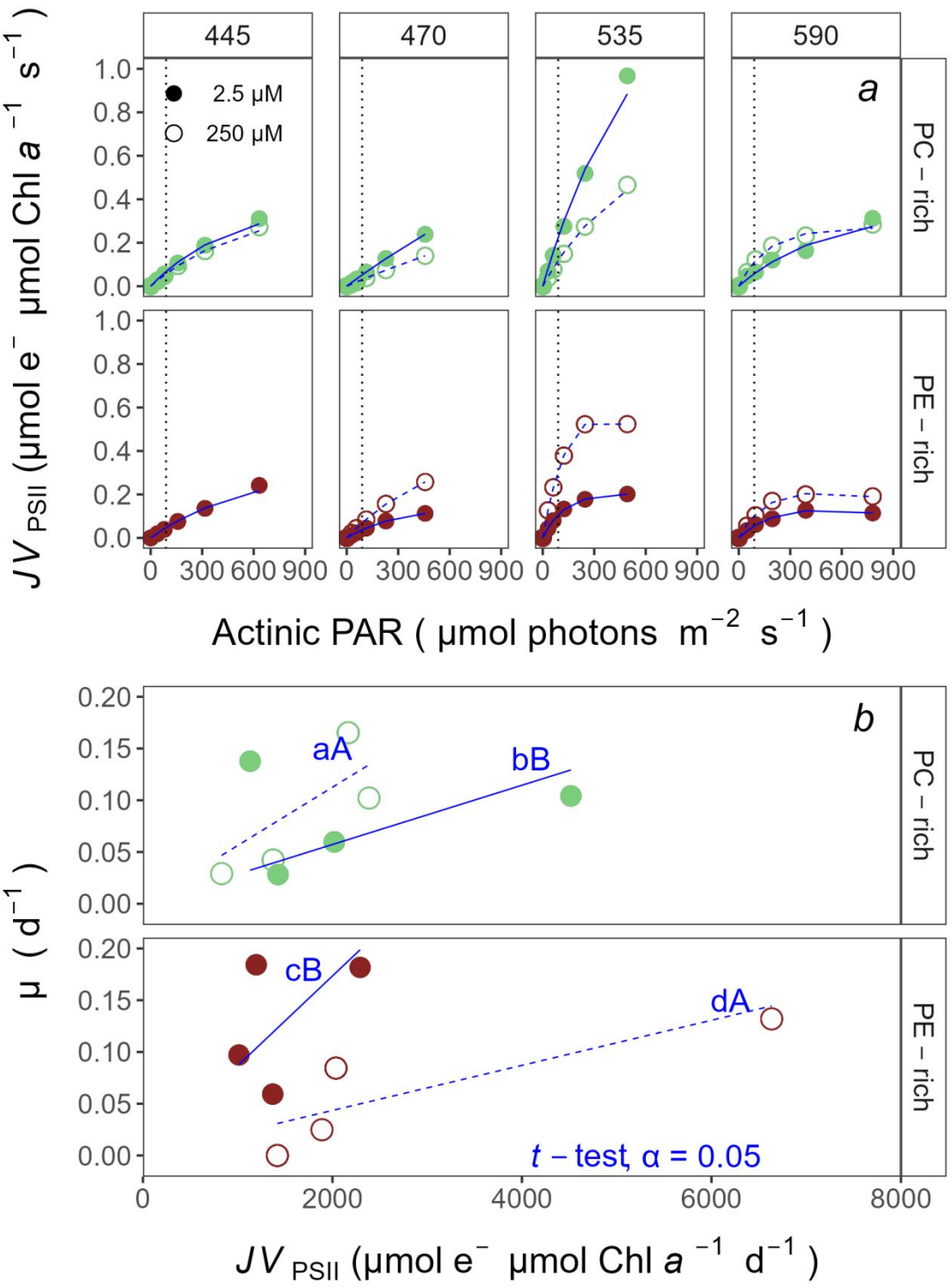

391

392 **Fig.** 4: PSII electron flux (JV_{PSII}; µmol e^- µmol Chl a^{-1} s^{-1}) vs. Actinic PAR (µmol photons $m^{-2}s^{-1}$)

393 (*a*). JV_{PSII} was estimated using FRRf induction curves with excitation at Ex_{445nm}, blue; Ex_{470nm},

394 blue-green; Ex_{535nm}, green; or Ex_{590nm}, orange; for PC-rich (green circle) or PE-rich (red circle)
395 cultures of *Synechococcus*. Data show situations in which cultures were excited by, and growing
396 in, corresponding growth wavebands of 450, 470, 530, or 620 nm and 250 µM [O_2] (open symbols
397 and dashed line) or 2.5 µM [O_2] (closed symbols and solid line). JV_{PSII} vs. Actinic PAR (µmol
398 photons $m^{-2}s^{-1}$) was fit with a Harrison and Platt Light Response Curve model (Harrison and Platt
399 1986), used to estimated JV_{PSII} at 90 µmol photons $m^{-2}s^{-1}$ (vertical dotted lines). Chlorophyll-
400 specific growth rates (µ; d^{-1}) vs. PSII electron flux (JV_{PSII}; µmol e^- µmol Chl a^{-1} d^{-1}) measured
401 under half (90 µmol photons $m^{-2}s^{-1}$) of diel peak PAR growth light (*b*). Blue lines (solid for 2.5
402 µM [O_2] or dashed for 250 µM O_2) show linear model fit for data from each strain across spectral
403 wavebands. Different blue lowercase letters indicate statistically significant differences between
404 the fit models for different [O_2] within a given strain. Different blue uppercase letters indicate
405 statistically significant differences between the fit models for different strains within a given [O_2]
406 (*t*-test; $p < 0.05$).
407

408 Discussion

409 Growth responses of PC-rich and PE-rich picocyanobacteria across [O_2] and spectral
410 wavebands

411 Picocyanobacteria from the genus *Synechococcus* are major contributors to primary marine
412 production, across a wide range of environments (Śliwińska-Wilczewska et al. 2018a; Aguilera et
413 al. 2023) but interactive influences of [O_2] and spectral wavebands on their growth rates and
414 ecophysiology have not yet been investigated.

415 PC-rich and PE-rich *Synechococcus* from coastal habitats are exposed to changes in
416 irradiance, spectral waveband, and sometimes [O_2], by vertical movements through the mixed

417 layer. Fluctuation in spectral wavebands changes the balance between productive photosynthesis,
418 and photoinactivation of PSII (Six et al. 2007), increasing the cost of growth by diverting protein
419 metabolism towards PSII repair (Murphy et al. 2017). Indeed, under 250 μM [O_2], the PC-rich
420 strain failed to grow under 405 nm, while the PE-rich strain failed to grow under 405 and 450,
421 consistent with accelerated photoinactivation of PSII under blue wavebands (Murphy et al. 2017).
422 In contrast, growth persisted in both strains at 405 & 450 nm under 2.5 μM [O_2], likely because
423 generation of toxic Reactive Oxygen Species (ROS) was suppressed, lowering the burden of
424 photoinactivation of PSII.

425 μ shows positive responses to both Phycobiliproteins:Chlorophyll *a* ratio, an index of light
426 capture capacity, and to cumulative diel PSII electron flux (JV_{PSII}) for *Synechococcus*, although
427 the relations varied across strain and with [O_2]. In the PC-rich strain lower [O_2] lowered the yield
428 of growth per electron flux, while in the PE-rich strain the yield of growth per electron flux
429 increased under lower [O_2]. Note that these regressions excluded those conditions where no growth
430 occurred. In contrast, growth showed no correlation to estimated Photosynthetically Usuable
431 Radiation (PUR) (Fig. S4), likely because of variable allocations of excitation from
432 phycobilisomes across growth conditions (Campbell 1996), not captured in the PUR metric based
433 upon light absorption.

434 Wong et al. (2023) found that vertical structures of phytoplankton communities in OMZ are
435 not sufficiently explained by top-down predation pressure nor light and/or nutrient limitation and
436 thus, some phytoplankton may have a higher than expected direct O_2 requirement, with growth
437 inhibited by low O_2 levels. However, in our work we show that low oxygen levels either do not
438 suppress, and sometimes even benefit, growth of strains representing different *Synechococcus*
439 pigment phenotypes across spectral wavebands. What is more, historical data link major extinction

events to warm climates and oxygen-deficient oceans, with current anthropogenic activities possibly leading to widespread OMZ within a thousand years (Breitburg et al. 2018). The PC-rich *Synechococcus* strain showed generally similar growth rates under high and low tested [O_2], while the PE-rich strain achieved faster growth rates under low (2.5 μM) than under high (250 μM) [O_2]. PE-rich *Synechococcus* are typically found at greater depths, and lower light, than are PC-rich strains (Haverkamp et al. 2009; Śliwińska-Wilczewska et al. 2018a) but we suggest that at least some PE-rich strains may actually be limited to lower light niches by the interactions between light level, spectral band, and full air-saturated [O_2]. In lower oxygen waters some PE-rich strains may exploit higher light niches nearer the surface.

Physiological adaptations of PC-rich and PE-rich picocyanobacteria to [O_2] and spectral wavebands

Synechococcus strains vary widely in pigment composition, enabling them to exploit different spectral niches (Moore et al. 1995; Six et al. 2007; Grébert et al. 2018; Efimova et al. 2020). With a small diameter of 0.8–2.0 μm, *Synechococcus* possess a high surface-to-volume ratio (Śliwińska-Wilczewska et al. 2018b), minimizing pigment package effects (Finkel 2001), and resulting in high optical absorption per pigment. This characteristic allows them to thrive under low light deep in the water column (Moore et al. 1995), and to disproportionately influence sub-surface light fields (Berthold and Schumann 2020). Although limited package effect increases photon capture per pigment investment, it also increases *Synechococcus* susceptibility to light-induced damage (Llabrés and Agustí 2006, 2010). In some *Synechococcus*, a carotenoid-protein complex regulates the connectivity of the phycobilisome to the reaction center, mediating a form of non-photochemical quenching of excitation (Wilson et al. 2006; Gorbunov et al. 2011;

463 Kirilovsky 2015). In our work we found no change in bulk carotenoids content (Fig. 2), nor in Car
464 to Chl *a* ratio (Fig. S3) under the different [O_2]. What is more, for the chosen PE-rich strain, the
465 carotenoids content did not change across tested wavebands. On the other hand, for the chosen PC-
466 rich strain, a slight increase in carotenoids content was recorded under 405 nm, although these
467 cells were not growing and were thus under stress.

468 σ_{PSII} was low and showed little change with increasing actinic light during excitation through
469 chlorophyll at Ex_{445nm}, because in cyanobacteria the number of chlorophyll per PSII is low, and
470 nearly fixed, so the effective absorption cross section of PSII for chlorophyll is low (Xu et al.
471 2018). With excitation through the phycobilisomes at 535 and 590 nm σ_{PSII} rose to a peak near the
472 acclimated light level of ~ 90 μmol photons $m^{-2}s^{-1}$ (Campbell and Oquist 1996), reflecting the
473 state transition from State II in the dark towards State I near the growth light level, with subsequent
474 decrease in σ_{PSII}, as excitation is again directed away from PSII.

475 τ_{PSII} was generally faster for both the chosen PC-rich and PE-rich strains under 250 μM [O_2],
476 consistent with the cyanobacterial capacity for pseudo-cyclic electron flows away from PSII to
477 [O_2] (Campbell et al. 1999; Grossman et al. 2010; Allahverdiyeva et al. 2015; Hughes et al. 2018),
478 thereby controlling feedback inhibition of electron transport. In parallel, q_P was generally higher
479 for the PC-rich, and particularly for the PE-rich strain, under 250 μM [O_2], since cyanobacteria
480 show strong capacity for electron flow away from PSII to O_2 (Campbell et al. 1999; Hughes et al.
481 2018), particularly under excess excitation above the acclimated PAR of ~ 90 μmol photons
482 $m^{-2}s^{-1}$. In spite of this faster electron transport performance under 250 μM [O_2] the PE-rich strain
483 grew faster under 2.5 μM [O_2], showing an increase in the growth return upon electron transport,
484 possibly because of a decrease in metabolic burden, through suppression of ROS formation under

lower [O_2]. Future genomic comparisons may uncover the bases for these distinct strain responses to changing [O_2].

Picocyanobacteria numerically dominate vast tracts of the oceans, contributing significant primary production, particularly in oligotrophic regions, but also some coastal habitats (Haverkamp 2008; Larsson et al. 2014; Doré et al. 2022; Aguilera et al. 2023). The ecological success of picoplanktonic *Synechococcus* reflects specific lineages occupying different niches to populate the world's oceans (Scanlan 2012). Picocyanobacteria species can share the light spectrum by specializing in different wavelengths (Stomp et al. 2004, 2007; Haverkamp et al. 2009). Competition models and laboratory experiments show that PE-rich picocyanobacteria outperform competitors in green light while PC-rich picocyanobacteria dominate in red light, while both species can coexist across the full spectrum (Stomp et al. 2004, 2007). We now find that spectral wavebands interact with [O_2] as determinants of growth rates across PE- and PC-rich strains of *Synechococcus*, and that changing ocean [O_2] might drive strains of different pigmentation phenotypes into changing ecological niches.

Acknowledgements

We would like to express our sincere gratitude to the Editor, and two Reviewers for their efforts reviewing and improving this manuscript. We thank Naaman M. Omar for assistance with coding, data analyses and culture maintenance; Miranda Corkum who maintained cultures and trained personnel in culture handling; Laurel Genge, and Carlie Barnhill (Mount Allison students) who assisted with R code.

Article information

Data availability statement

Data supporting this study is available on: https://github.com/FundyPhytoPhys/BalticO2 (public GitHub Repository) and https://docs.google.com/spreadsheets/d/1ZXpwR7Gfto-uRzVdXzMpQF4frbrvMLH_IyLqonFZRSw/edit#gid=0 (URL for MetaDataCatalog).

Code to perform data processing and analyses is available at https://github.com/FundyPhytoPhys/BalticO2.

Author information

Author ORCIDs

Sylwia Śliwińska-Wilczewska https://orcid.org/0000-0002-3147-6605 Mireille Savoie https://orcid.org/0009-0009-9499-6657 Douglas A. Campbell https://orcid.org/0000-0001-8996-5463

Author contributions

Conceptualization: SSW, DAC Data curation: SSW Formal analysis: SSW, MS, DAC Funding acquisition: DAC Investigation: SSW Methodology: SSW, MS, DAC Project administration: DAC Resources: DAC Supervision: DAC Validation: SSW, MS, DAC Visualization: SSW Writing – original draft: SSW, MS, DAC

Competing interests

The authors declare there are no competing interests.

Funding information

This work was supported by Canada Research Chair in Phytoplankton Ecophysiology (DAC) and Latitude & Light; NSERC of Canada Discovery Grant (DAC).

Supplementary material

Supplementary data are available with the article at https: //github.com/FundyPhytoPhys/BalticO2.

References

Aguilera, A., Alegria Zufia, J., Bas Conn, L., Gurlit, L., Śliwińska-Wilczewska, S., Budzałek, G., Lundin, D., Pinhassi, J., Legrand, C., and Farnelid, H. 2023. Ecophysiological analysis reveals distinct environmental preferences in closely related Baltic Sea picocyanobacteria. Environmental Microbiology **25**(9): 1674–1695. doi:10.1111/1462-2920.16384.

Allahverdiyeva, Y., Isojärvi, J., Zhang, P., and Aro, E.-M. 2015. Cyanobacterial Oxygenic Photosynthesis is Protected by Flavodiiron Proteins. Life **5**(1): 716–743. Multidisciplinary Digital Publishing Institute. doi:10.3390/life5010716.

Andersson, B., Salter, A.H., Virgin, I., Vass, I., and Styring, S. 1992. Photodamage to photosystem II - primary and secondary events. Journal of Photochemistry and Photobiology B: Biology **15**(1): 15–31. doi:10.1016/1011-1344(92)87003-R.

Bagby, S.C., and Chisholm, S.W. 2015. Response of Prochlorococcus to varying CO2:O2 ratios. The ISME Journal **9**(10): 2232–2245. doi:10.1038/ismej.2015.36.

551 Bennett, A., and Bogorad, L. 1973. Complementary Chromatic Adaptation in a filamentous blue-
552 green alga. Journal of Cell Biology **58**(2): 419–435. doi:10.1083/jcb.58.2.419.

553 Berthold, M., and Schumann, R. 2020. Phosphorus Dynamics in a Eutrophic Lagoon: Uptake and
554 Utilization of Nutrient Pulses by Phytoplankton. Frontiers in Marine Science **7**. Frontiers.
555 doi:10.3389/fmars.2020.00281.

556 Blake, R., and Griff, M. 2012. In situ spectroscopy on intact *Leptospirillum Ferrooxidans* reveals
557 that reduced cytochrome 579 is an obligatory intermediate in the aerobic iron respiratory chain.
558 Frontiers in Microbiology **3**. [accessed 13 June 2023].

559 Boatman, T.G., Geider, R.J., and Oxborough, K. 2019. Improving the accuracy of Single Turnover
560 Active Fluorometry (STAF) for the estimation of Phytoplankton Primary Productivity (PhytoPP).
561 Frontiers in Marine Science **6**. Frontiers. doi:10.3389/fmars.2019.00319.

562 Breitburg, D., Levin, L.A., Oschlies, A., Grégoire, M., Chavez, F.P., Conley, D.J., Garçon, V.,
563 Gilbert, D., Gutiérrez, D., Isensee, K., Jacinto, G.S., Limburg, K.E., Montes, I., Naqvi, S.W.A.,
564 Pitcher, G.C., Rabalais, N.N., Roman, M.R., Rose, K.A., Seibel, B.A., Telszewski, M., Yasuhara,
565 M., and Zhang, J. 2018. Declining oxygen in the global ocean and coastal waters. Science
566 **359**(6371): eaam7240. American Association for the Advancement of Science.
567 doi:10.1126/science.aam7240.

568 Callieri, C., Cabello-Yeves, P.J., and Bertoni, F. 2022. The "Dark Side" of Picocyanobacteria: Life
569 as We Do Not Know It (Yet). Microorganisms **10**(3): 546. Multidisciplinary Digital Publishing
570 Institute. doi:10.3390/microorganisms10030546.

571 Campbell, D. 1996. Complementary chromatic adaptation alters photosynthetic strategies in the
572 cyanobacterium Calothrix. Microbiology **142**(5): 1255–1263. Microbiology Society,.
573 doi:10.1099/13500872-142-5-1255.

574 Campbell, D., Clarke, A.K., Gustafsson, P., and Öquist, G. 1999. Oxygen-dependent electron flow
575 influences photosystem II function and psbA gene expression in the cyanobacterium
576 Synechococcus sp. PCC 7942. Physiologia Plantarum **105**(4): 746–755. doi:10.1034/j.1399-
577 3054.1999.105420.x.

578 Campbell, D., and Oquist, G. 1996. Predicting Light Acclimation in Cyanobacteria from
579 Nonphotochemical Quenching of Photosystem II Fluorescence, Which Reflects State Transitions
580 in These Organisms. Plant Physiology **111**(4): 1293–1298. doi:10.1104/pp.111.4.1293.

581 Doré, H., Leconte, J., Guyet, U., Breton, S., Farrant, G.K., Demory, D., Ratin, M., Hoebeke, M.,
582 Corre, E., Pitt, F.D., Ostrowski, M., Scanlan, D.J., Partensky, F., Six, C., and Garczarek, L. 2022.
583 Global Phylogeography of Marine Synechococcus in Coastal Areas Reveals Strong Community
584 Shifts. mSystems **7**(6): e00656–22. American Society for Microbiology.
585 doi:10.1128/msystems.00656-22.

586 Efimova, T.V., Churilova, T.Ya., and Mukhanov, V.S. 2020. The Influence of Light of Different
587 Spectral Qualities on the Photosynthetic Characteristics of C-Phycocyanine-Containing
588 Cyanobacteria Synechococcus sp. WH5701. Russian Journal of Marine Biology **46**(2): 105–112.
589 doi:10.1134/S1063074020020042.

590 Elzhov, T.V., Mullen, K.M., Spiess, A.-N., and Bolker, B. 2023, September. Minpack.lm: R
591 Interface to the Levenberg-Marquardt Nonlinear Least-Squares Algorithm Found in MINPACK,
592 Plus Support for Bounds. [accessed 15 March 2024].

593 Falkowski, P.G., Katz, M.E., Knoll, A.H., Quigg, A., Raven, J.A., Schofield, O., and Taylor, F.J.R.
594 2004. The Evolution of Modern Eukaryotic Phytoplankton. Science **305**(5682): 354–360.
595 American Association for the Advancement of Science. doi:10.1126/science.1095964.

596 Falkowski, P., and Kolber, Z. 1993. Estimation of phytoplankton photosynthesis by active
597 fluorescence. ICES Marine Science Symposium **197**: 92–103.

598 Finkel, Z.V. 2001. Light absorption and size scaling of light-limited metabolism in marine
599 diatoms. Limnology and Oceanography **46**(1): 86–94. doi:10.4319/lo.2001.46.1.0086.

600 Flombaum, P., Gallegos, J.L., Gordillo, R.A., Rincón, J., Zabala, L.L., Jiao, N., Karl, D.M., Li,
601 W.K.W., Lomas, M.W., Veneziano, D., Vera, C.S., Vrugt, J.A., and Martiny, A.C. 2013. Present
602 and future global distributions of the marine Cyanobacteria *Prochlorococcus* and *Synechococcus*.
603 Proceedings of the National Academy of Sciences **110**(24): 9824–9829. Proceedings of the
604 National Academy of Sciences. doi:10.1073/pnas.1307701110.

605 Gorbunov, M.Y., Kuzminov, F.I., Fadeev, V.V., Kim, J.D., and Falkowski, P.G. 2011. A kinetic
606 model of non-photochemical quenching in cyanobacteria. Biochimica et Biophysica Acta (BBA)
607 - Bioenergetics **1807**(12): 1591–1599. doi:10.1016/j.bbabio.2011.08.009.

608 Grébert, T., Doré, H., Partensky, F., Farrant, G.K., Boss, E.S., Picheral, M., Guidi, L., Pesant, S.,
609 Scanlan, D.J., Wincker, P., Acinas, S.G., Kehoe, D.M., and Garczarek, L. 2018. Light color
610 acclimation is a key process in the global ocean distribution of Synechococcus cyanobacteria.
611 Proceedings of the National Academy of Sciences **115**(9): E2010–E2019. Proceedings of the
612 National Academy of Sciences. doi:10.1073/pnas.1717069115.

Grossman, A.R., Mackey, K.R.M., and Bailey, S. 2010. A Perspective on Photosynthesis in the Oligotrophic Oceans: Hypotheses Concerning Alternate Routes of Electron Flow1. Journal of Phycology **46**(4): 629–634. doi:10.1111/j.1529-8817.2010.00852.x.

Guillard, R.R.L. 1975. Culture of phytoplankton for feeding marine invertebrates. *In* Culture of Marine Invertebrate Animals: Proceedings — 1st Conference on Culture of Marine Invertebrate Animals Greenport. *Edited by* W.L. Smith and M.H. Chanley. Springer US, Boston, MA. pp. 29–60. doi:10.1007/978-1-4615-8714-9_3.

Hakala, M., Tuominen, I., Keränen, M., Tyystjärvi, T., and Tyystjärvi, E. 2005. Evidence for the role of the oxygen-evolving manganese complex in photoinhibition of Photosystem II. Biochimica et Biophysica Acta (BBA) - Bioenergetics **1706**(1): 68–80. doi:10.1016/j.bbabio.2004.09.001.

Handel, A. 2020, October. Andreas Handel - Custom Word formatting using R Markdown. https://www.andreashandel.com/posts/2020-10-07-custom-word-format/. [accessed 13 June 2023].

Harrison, W.G., and Platt, T. 1986. Photosynthesis-irradiance relationships in polar and temperate phytoplankton populations. Polar biology **5**: 153–164. Springer. [accessed 15 March 2024].

Haverkamp, T.H.A. 2008. Shades of red and green : The colorful diversity and ecology of picocyanobacteria in the Baltic Sea. YersekeNetherlands Institute of Ecology (NIOO) - Royal Netherlands Academy of Arts and Sciences. [accessed 3 July 2024].

Haverkamp, T.H.A., Schouten, D., Doeleman, M., Wollenzien, U., Huisman, J., and Stal, L.J. 2009. Colorful microdiversity of Synechococcus strains (picocyanobacteria) isolated from the Baltic Sea. The ISME Journal **3**(4): 397–408. doi:10.1038/ismej.2008.118.

634 Hughes, D.J., Campbell, D.A., Doblin, M.A., Kromkamp, J.C., Lawrenz, E., Moore, C.M.,
635 Oxborough, K., Prášil, O., Ralph, P.J., Alvarez, M.F., and Suggett, D.J. 2018. Roadmaps and
636 Detours: Active Chlorophyll-a Assessments of Primary Productivity Across Marine and
637 Freshwater Systems. Environmental Science & Technology **52**(21): 12039–12054. American
638 Chemical Society. doi:10.1021/acs.est.8b03488.

639 Jávorfi, T., Erostyák, J., Gál, J., Buzády, A., Menczel, L., Garab, G., and Razi Naqvi, K. 2006.
640 Quantitative spectrophotometry using integrating cavities. Journal of Photochemistry and
641 Photobiology B: Biology **82**(2): 127–131. doi:10.1016/j.jphotobiol.2005.10.002.

642 Keeling, R.F., Körtzinger, A., and Gruber, N. 2010. Ocean Deoxygenation in a Warming World.
643 Annual Review of Marine Science **2**(Volume 2, 2010): 199–229. Annual Reviews.
644 doi:10.1146/annurev.marine.010908.163855.

645 Kirilovsky, D. 2015. Modulating energy arriving at photochemical reaction centers: Orange
646 carotenoid protein-related photoprotection and state transitions. Photosynthesis Research **126**(1):
647 3–17. doi:10.1007/s11120-014-0031-7.

648 Kolber, Z.S., Prášil, O., and Falkowski, P.G. 1998. Measurements of variable chlorophyll
649 fluorescence using fast repetition rate techniques: Defining methodology and experimental
650 protocols. Biochimica et Biophysica Acta (BBA) - Bioenergetics **1367**(1): 88–106.
651 doi:10.1016/S0005-2728(98)00135-2.

652 Larsson, J., Celepli, N., Ininbergs, K., Dupont, C.L., Yooseph, S., Bergman, B., and Ekman, M.
653 2014. Picocyanobacteria containing a novel pigment gene cluster dominate the brackish water
654 Baltic Sea. The ISME Journal **8**(9): 1892–1903. doi:10.1038/ismej.2014.35.

Latala, A., Jodlowska, S., and Pniewski, F. 2006. Culture Collection of Baltic Algae (CCBA) and characteristic of some strains by factorial experiment approach. Archiv fur Hydrobiologie **122**: 137–154. [accessed 19 June 2024].

Llabrés, M., and Agustí, S. 2006. Picophytoplankton cell death induced by UV radiation: Evidence for oceanic Atlantic communities. Limnology and Oceanography **51**(1): 21–29. doi:10.4319/lo.2006.51.1.0021.

Llabrés, M., and Agustí, S. 2010. Effects of ultraviolet radiation on growth, cell death and the standing stock of Antarctic phytoplankton. Aquatic Microbial Ecology **59**(2): 151–160. doi:10.3354/ame01392.

Luimstra, V.M., Schuurmans, J.M., Verschoor, A.M., Hellingwerf, K.J., Huisman, J., and Matthijs, H.C.P. 2018. Blue light reduces photosynthetic efficiency of cyanobacteria through an imbalance between photosystems I and II. Photosynthesis Research **138**(2): 177–189. doi:10.1007/s11120-018-0561-5.

Moore, L.R., Goericke, R., and Chisholm, S.W. 1995. Comparative physiology of Synechococcus and Prochlorococcus: Influence of light and temperature on growth, pigments, fluorescence and absorptive properties. Marine Ecology Progress Series **116**(1/3): 259–275. Inter-Research Science Center. Available from https://www.jstor.org/stable/44635011 [accessed 1 July 2024].

Morel, A. 1978. Available, usable, and stored radiant energy in relation to marine photosynthesis. Deep Sea Research **25**(8): 673–688. doi:10.1016/0146-6291(78)90623-9.

674 Murphy, C.D., Roodvoets, M.S., Austen, E.J., Dolan, A., Barnett, A., and Campbell, D.A. 2017.
675 Photoinactivation of Photosystem II in Prochlorococcus and Synechococcus. PLOS ONE **12**(1):
676 e0168991. Public Library of Science. doi:10.1371/journal.pone.0168991.

677 Oxborough, K., and Baker, N.R. 1997. Resolving chlorophyll *a* fluorescence images of
678 photosynthetic efficiency into photochemical and non-photochemical components – calculation of
679 qP and Fv-/Fm-; without measuring Fo-; Photosynthesis Research **54**(2): 135–142.
680 doi:10.1023/A:1005936823310.

681 Oxborough, K., Moore, C.M., Suggett, D.J., Lawson, T., Chan, H.G., and Geider, R.J. 2012. Direct
682 estimation of functional PSII reaction center concentration and PSII electron flux on a volume
683 basis: A new approach to the analysis of Fast Repetition Rate fluorometry (FRRf) data. Limnology
684 and Oceanography: Methods **10**(3): 142–154. doi:10.4319/lom.2012.10.142.

685 Partensky, F., Mella-Flores, D., Six, C., Garczarek, L., Czjzek, M., Marie, D., Kotabová, E.,
686 Felcmanová, K., and Prášil, O. 2018. Comparison of photosynthetic performances of marine
687 picocyanobacteria with different configurations of the oxygen-evolving complex. Photosynthesis
688 Research **138**(1): 57–71. doi:10.1007/s11120-018-0539-3.

689 Pedersen, T.L. 2024, January. Patchwork: The Composer of Plots. [accessed 20 April 2024].

690 Posit team. 2022. RStudio: Integrated development environment for r. Posit Software, PBC,
691 Boston, MA. Available from http://www.posit.co/.

692 R Core Team. 2023. R: A language and environment for statistical computing. R Foundation for
693 Statistical Computing, Vienna, Austria. Available from https://www.R-project.org/.

694 Scanlan, D.J. 2012. Marine Picocyanobacteria. *In* Ecology of Cyanobacteria II: Their Diversity in
695 Space and Time. *Edited by* B.A. Whitton. Springer Netherlands, Dordrecht. pp. 503–533.
696 doi:10.1007/978-94-007-3855-3_20.

697 Six, C., Finkel, Z.V., Irwin, A.J., and Campbell, D.A. 2007. Light variability illuminates niche-
698 partitioning among marine picocyanobacteria. PLOS ONE **2**(12): e1341. Public Library of
699 Science. doi:10.1371/journal.pone.0001341.

700 Śliwińska-Wilczewska, S., Cieszyńska, A., Maculewicz, J., and Latała, A. 2018a.
701 Ecophysiological characteristics of red, green, and brown strains of the Baltic picocyanobacterium
702 *Synechococcus* sp. – a laboratory study. Biogeosciences **15**(20): 6257–6276. Copernicus GmbH.
703 doi:10.5194/bg-15-6257-2018.

704 Śliwińska-Wilczewska, S., Maculewicz, J., Barreiro Felpeto, A., and Latała, A. 2018b.
705 Allelopathic and bloom-forming picocyanobacteria in a changing world. Toxins **10**(1): 48.
706 Multidisciplinary Digital Publishing Institute. doi:10.3390/toxins10010048.

707 Stomp, M., Huisman, J., de Jongh, F., Veraart, A.J., Gerla, D., Rijkeboer, M., Ibelings, B.W.,
708 Wollenzien, U.I.A., and Stal, L.J. 2004. Adaptive divergence in pigment composition promotes
709 phytoplankton biodiversity. Nature **432**(7013): 104–107. Nature Publishing Group.
710 doi:10.1038/nature03044.

711 Stomp, M., Huisman, J., Vörös, L., Pick, F.R., Laamanen, M., Haverkamp, T., and Stal, L.J. 2007.
712 Colourful coexistence of red and green picocyanobacteria in lakes and seas. Ecology Letters **10**(4):
713 290–298. doi:10.1111/j.1461-0248.2007.01026.x.

714 Strickland, J.D., and Parsons, T.R. 1972. Practical Hand Book of Seawater Analysis. Fisheries
715 Research Board of Canada **167 (2nd edition)**: 1–311. doi:DOI: http://dx.doi.org/10.25607/OBP-
716 1791.

717 Tortell, P., and Suggett, D.J. 2021. A user guide for the application of Single Turnover active
718 chlorophyll fluorescence for phytoplankton productivity measurements. Version 1. Report,
719 Scientific Committee on Oceanic Research (SCOR) Working Group 156. doi:10.25607/OBP-
720 1084.

721 Ulloa, O., Canfield, D.E., DeLong, E.F., Letelier, R.M., and Stewart, F.J. 2012. Microbial
722 oceanography of anoxic oxygen minimum zones. Proceedings of the National Academy of
723 Sciences **109**(40): 15996–16003. Proceedings of the National Academy of Sciences.
724 doi:10.1073/pnas.1205009109.

725 Ulloa, O., Henríquez-Castillo, C., Ramírez-Flandes, S., Plominsky, A.M., Murillo, A.A., Morgan-
726 Lang, C., Hallam, S.J., and Stepanauskas, R. 2021. The cyanobacterium Prochlorococcus has
727 divergent light-harvesting antennae and may have evolved in a low-oxygen ocean. Proceedings of
728 the National Academy of Sciences **118**(11): e2025638118. Proceedings of the National Academy
729 of Sciences. doi:10.1073/pnas.2025638118.

730 Wickham, H. 2016. Data Analysis. *In* Ggplot2: Elegant Graphics for Data Analysis. *Edited by* H.
731 Wickham. Springer International Publishing, Cham. pp. 189–201. doi:10.1007/978-3-319-24277-
732 4_9.

733 Wilson, A., Ajlani, G., Verbavatz, J.-M., Vass, I., Kerfeld, C.A., and Kirilovsky, D. 2006. A
734 Soluble Carotenoid Protein Involved in Phycobilisome-Related Energy Dissipation in
735 Cyanobacteria. The Plant Cell **18**(4): 992–1007. doi:10.1105/tpc.105.040121.

736 Wlodkowic, D., Czerw, A., Karakiewicz, B., and Deptała, A. 2022. Recent progress in cytometric
737 technologies and their applications in ecotoxicology and environmental risk assessment.
738 Cytometry Part A **101**(3): 203–219. doi:10.1002/cyto.a.24508.

739 Wong, J.C.Y., Raven, J.A., Aldunate, M., Silva, S., Gaitán-Espitia, J.D., Vargas, C.A., Ulloa, O.,
740 and von Dassow, P. 2023. Do phytoplankton require oxygen to survive? A hypothesis and model
741 synthesis from oxygen minimum zones. Limnology and Oceanography **68**(7): 1417–1437.
742 doi:10.1002/lno.12367.

743 Xu, K., Grant-Burt, J.L., Donaher, N., and Campbell, D.A. 2017. Connectivity among
744 Photosystem II centers in phytoplankters: Patterns and responses. Biochimica et Biophysica Acta
745 (BBA) - Bioenergetics **1858**(6): 459–474. doi:10.1016/j.bbabio.2017.03.003.

746 Xu, K., Lavaud, J., Perkins, R., Austen, E., Bonnanfant, M., and Campbell, D.A. 2018.
747 Phytoplankton σPSII and excitation dissipation; implications for estimates of primary
748 productivity. Frontiers in Marine Science **5**. doi:10.3389/fmars.2018.00281.

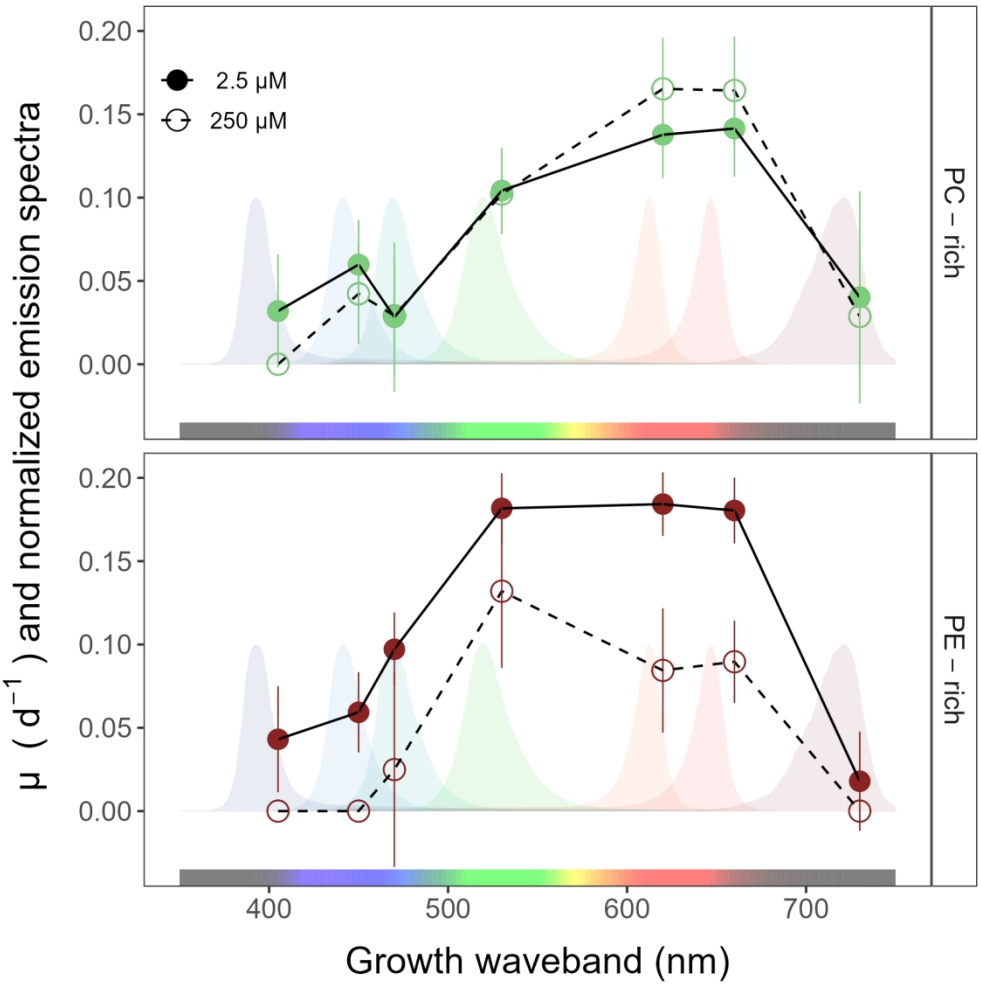

Fig. 1. Chlorophyll-specific growth rates (µ; d−1) vs. growth waveband (nm, shaded regions). Growth rates (± SE) were estimated from logistic fits of chlorophyll proxy OD680 – OD720 (ΔOD) vs. elapsed time (Fig. S1), for PC-rich (green circle) and PE-rich (red circle) cultures of Synechococcus grown at spectral wavebands of 405, 450, 470, 530, 620, 660, or 730 nm, and [O2] of 250 µM (open symbols and dashed line) or 2.5 µM (closed symbols and solid line).

387x387mm (118 x 118 DPI)

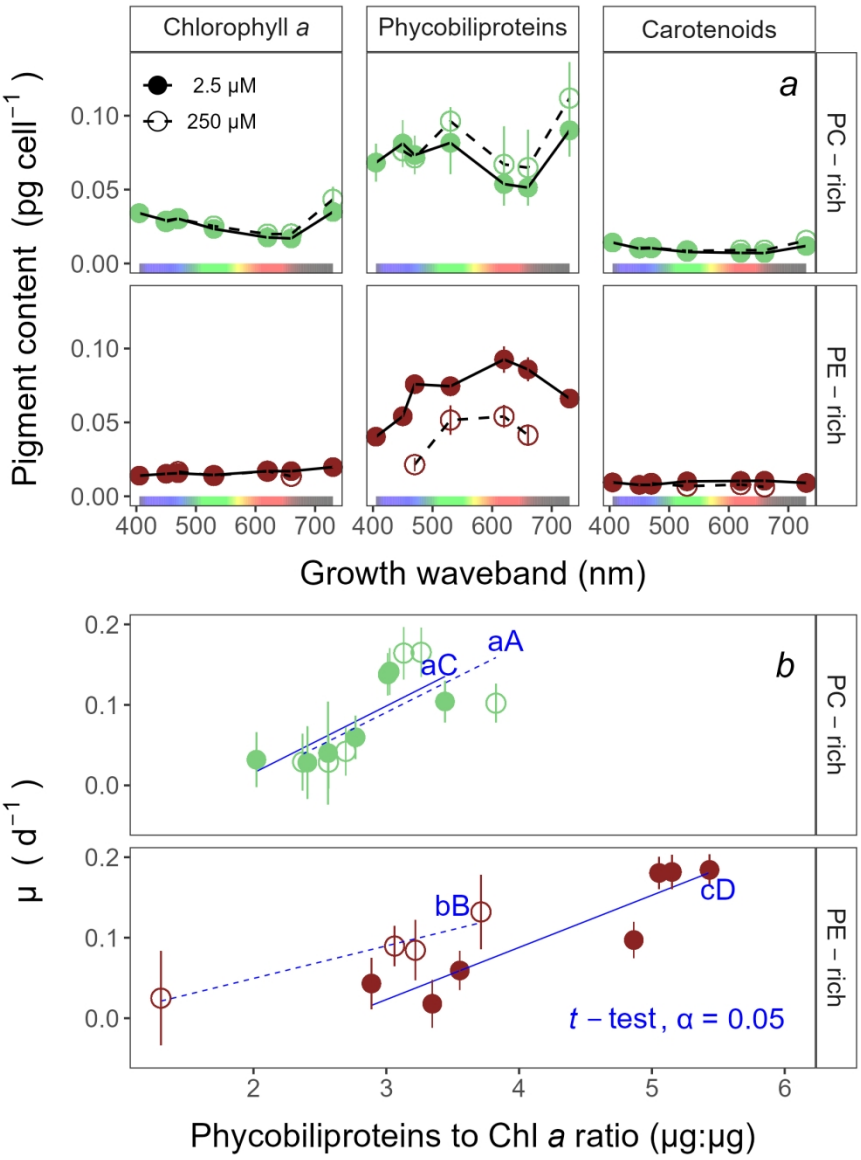

Fig. 2. Pigment content (pg cell −1) vs. growth waveband (nm) (a) and Chlorophyll-specific growth rates (µ; d−1) vs. Phycobiliproteins:Chlorophyll a ratio (µg:µg) (b) for PC-rich (green circle) and PE-rich (red circle) cultures of Synechococcus grown at spectral wavebands of 405, 450, 470, 530, 620, 660, or 730 nm and 250 µM [O2] (open symbols and dashed line) or 2.5 µM [O2] (closed symbols and solid line). Data not presented for those PE-rich cultures which showed negligible growth under 405, 450, 730 nm and 250 µM [O2]; nor for those PC-rich cultures which showed negligible growth under 405 nm and 250 µM [O2]. Blue lines show linear model fit for data from each strain and [O2] (solid for 2.5 µM [O2] or dashed for 250 µM [O2]) across spectral wavebands. Different blue lowercase letters indicate statistically significant differences between the fit models for different [O2] within a given strain. Different blue uppercase letters indicate statistically significant differences between the fit models for different strains within a given [O2] (t-test; $p < 0.05$).

387x516mm (118 x 118 DPI)

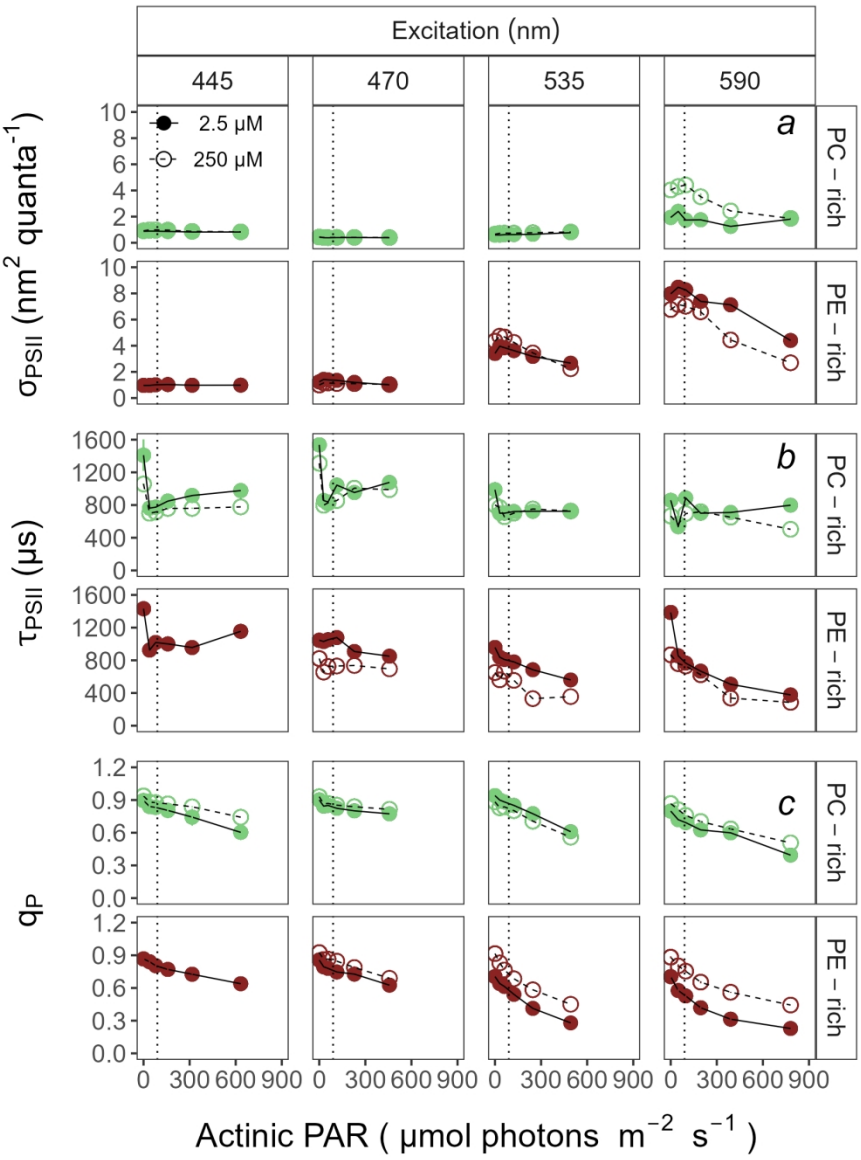

Fig. 3. Effective absorption cross section of PSII (σPSII; nm2 quanta−1) (a); turnover time of PSII photochemistry (τPSII; µs) (b); or photochemical quenching coefficient (qP) (c) vs. Actinic PAR (µmol photons m−2s−1). Parameters were estimated using FRRf induction curves with excitation (columns) at Ex445nm, blue; Ex470nm, blue-green; Ex535nm, green; or Ex590nm, orange; for PC-rich (green circle) or PE-rich (red circle) cultures of Synechococcus. Data show situations in which cultures were excited by, and growing in, corresponding growth wavebands of 450, 470, 530, or 620 nm and 250 µM [O2] (open symbols and dashed line) or 2.5 µM [O2] (closed symbols and solid line). The vertical lines show half diel peak PAR growth light of 90 µmol photons m−2s−1. Data not presented for those PE-rich cultures which showed negligible growth under 405, 450, 730 nm and 250 µM [O2]; nor for those PC-rich cultures which showed negligible growth under 405 nm and 250 µM [O2].

387x516mm (118 x 118 DPI)

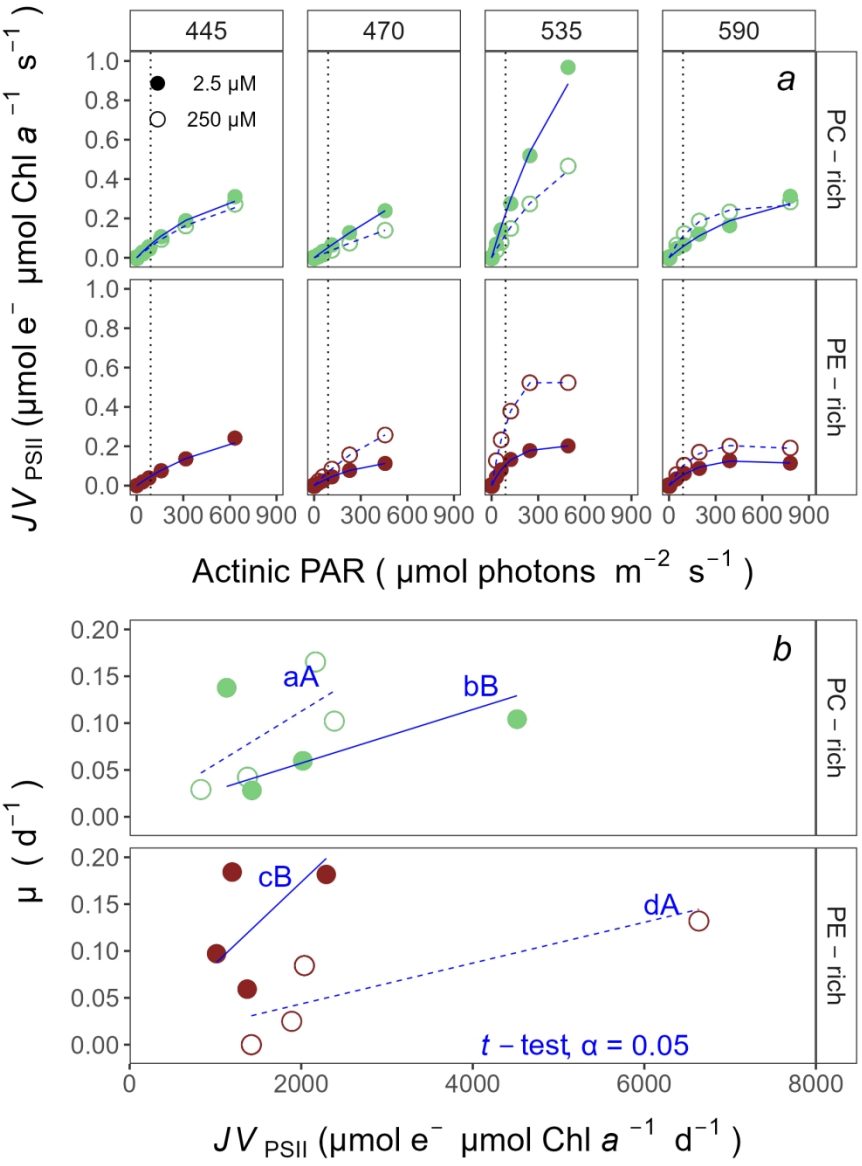

Fig. 4. PSII electron flux (JVPSII; µmol e− µmol Chl a−1 s−1) vs. Actinic PAR (µmol photons m−2s−1) (a). JVPSII was estimated using FRRf induction curves with excitation at Ex445nm, blue; Ex470nm, blue-green; Ex535nm, green; or Ex590nm, orange; for PC-rich (green circle) or PE-rich (red circle) cultures of Synechococcus. Data show situations in which cultures were excited by, and growing in, corresponding growth wavebands of 450, 470, 530, or 620 nm and 250 µM [O2] (open symbols and dashed line) or 2.5 µM [O2] (closed symbols and solid line). JVPSII vs. Actinic PAR (µmol photons m−2s−1) was fit with a Harrison and Platt Light Response Curve model (Harrison and Platt 1986), used to estimated JVPSII at 90 µmol photons m−2s−1 (vertical dotted lines). Chlorophyll-specific growth rates (µ; d−1) vs. PSII electron flux (JVPSII; µmol e− µmol Chl a−1 d−1) measured under half (90 µmol photons m−2s−1) of diel peak PAR growth light (b). Blue lines (solid for 2.5 µM [O2] or dashed for 250 µM O2) show linear model fit for data from each strain across spectral wavebands. Different blue lowercase letters indicate statistically significant differences between the fit models for different [O2] within a given strain. Different blue uppercase letters indicate statistically significant differences between the fit models for different strains within a given [O2] (t-test; $p < 0.05$).

387x516mm (118 x 118 DPI)